Rational combination therapy for hepatocellular carcinoma with PARP1 and DNA-PK inhibitors

Chen Wang[a,b,c,1], Huanyin Tang[a,1], Anke Geng[a,1], Binghua Dai[d,1], Haiping Zhang[a], Xiaoxiang Sun[a], Yu Chen[a], Zhibing Qiao[a], Hong Zhu[e], Jiamei Yang[d], Jiayu Chen[a], Qizhi He[a], Nan Qin[a], Jinru Xie[f], Rong Tan[f], Xiaoping Wan[a], Shaorong Gao[a], Ying Jiang[a,2], Fang-Lin Sun[b,g,2], and Zhiyong Mao[a,g,2]

[a]Clinical and Translational Research Center of Shanghai First Maternity & Infant Hospital, Shanghai Key Laboratory of Signaling and Disease Research, Frontier Science Center for Stem Cell Research, School of Life Sciences and Technology, Tongji University, Shanghai 200092, China; [b]Research Center for Translational Medicine at East Hospital, Advanced Institute of Translational Medicine, Tongji University, Shanghai 200092, China; [c]United Nations Environment Programme–Tongji Institute of Environment for Sustainable Development, Tongji University, Shanghai 200092, China; [d]Department of Special Treatment and Liver Transplantation, Shanghai Eastern Hepatobiliary Surgery Hospital, Shanghai 200438, China; [e]College of Pharmaceutical Sciences, Zhejiang University, Hangzhou, Zhejiang 310058, China; [f]Key Laboratory of Molecular Radiation Oncology Hunan Province, Xiangya Hospital, Central South University, Changsha 410008, China; and [g]Tsingtao Advanced Research Institute, Tongji University, Qingdao 266071, China

Edited by Christopher Hine, Cleveland Clinic, Cleveland, OH, and accepted by Editorial Board Member James E. Cleaver August 25, 2020 (received for review February 19, 2020)

Understanding differences in DNA double-strand break (DSB) repair between tumor and normal tissues would provide a rationale for developing DNA repair-targeted cancer therapy. Here, using knock-in mouse models for measuring the efficiency of two DSB repair pathways, homologous recombination (HR) and nonhomologous end-joining (NHEJ), we demonstrated that both pathways are up-regulated in hepatocellular carcinoma (HCC) compared with adjacent normal tissues due to altered expression of DNA repair factors, including PARP1 and DNA-PKcs. Surprisingly, inhibiting PARP1 with olaparib abrogated HR repair in HCC. Mechanistically, inhibiting PARP1 suppressed the clearance of nucleosomes at DNA damage sites by blocking the recruitment of ALC1 to DSB sites, thereby inhibiting RPA2 and RAD51 recruitment. Importantly, combining olaparib with NU7441, a DNA-PKcs inhibitor that blocks NHEJ in HCC, synergistically suppressed HCC growth in both mice and HCC patient-derived-xenograft models. Our results suggest the combined inhibition of both HR and NHEJ as a potential therapy for HCC.

DNA double-strand break repair | knock-in mouse models | clinical analysis | olaparib | NU7441

Hepatocellular carcinoma (HCC) is the sixth most common cancer and the second leading cause of cancer-related death worldwide, accounting for ∼600,000 deaths annually (1). Owing to the difficulty of early diagnosis, the shortage of organs for orthotopic liver transplantation, and the lack of effective targeted therapeutic methods, the mortality rate of HCC remains high. For instance, in the United States, the 1-y survival for HCC patients is <50%, and the 5-y overall survival is only ∼10% (2). Therefore, there is an urgent need for new therapeutic methods for curing HCC.

Two independent and competitive pathways, homologous recombination (HR) and nonhomologous end-joining (NHEJ), operate to ensure genome integrity by repairing DNA double-strand breaks (DSBs), the most detrimental type of DNA damage (3). NHEJ is further categorized into two subpathways, canonical NHEJ (c-NHEJ) and alternative NHEJ (alt-NHEJ) (4). Defects in these pathways may lead to increased rates of mutations and chromosomal rearrangements, which may occur on oncogenes or tumor suppressor genes and provide a survival advantage to tumor cells (5, 6). Similar to many other types of cancers, increased genomic instability is a potential driver of HCC (7, 8). However, theoretically, hyperactivated DSB repair by HR or/and NHEJ in cancer cells may support tumor maintenance, as constantly proliferating cancer cells need to cope with large amounts of DNA damage induced by high replication stress and increased levels of oxidative stress (9, 10).

Since the aim of HCC therapy is to selectively eliminate HCC cells with no or minimal damage to normal hepatocytes, the dual roles of DSB repair in cancer prevention and development complicates the potential clinical applications of small molecules targeting DSB repair. Therefore, understanding the differences in DSB repair capacity between HCC and normal tissues would help achieve the goal of developing a successful DSB repair targeting therapeutic strategy. However, due to the lack of mouse models for in vivo analysis of the differences in DSB repair capacity between HCC and adjacent normal tissues, whether DNA repair pathways can be targeted for HCC treatment has not been assessed.

The successful application of PARP1 inhibitors in treating *BRCA1/2*-deficient cancer is a classic example of rational development of DNA repair-targeted cancer therapy (11). Along with the considerable attention that has been given to PARP inhibitors as a monotherapy in treating HR-deficient cancers, great effort has been expended to explore the potential of PARP inhibitors in a various types of cancers both as single agents and in combination with other therapeutic methods (12, 13). Intriguingly, recent work has shown that the functions of PARP1 in DNA repair are not limited to fixing single-strand breaks; PARP1 is also recruited to DSB sites and participates in alt-NHEJ in a catalytic activity-dependent

Significance

Hepatocellular carcinoma (HCC) is the sixth most common type of cancer, and its mortality rate continues to increase. We generated knock-in reporter mouse models for measuring DNA double-strand break (DSB) repair efficiency and demonstrated that both DSB repair pathways are up-regulated in mouse HCCs. We then found that activation of PARP1 and DNA-PKcs is critical to HCC survival both in vitro and in vivo. Targeting the two proteins to block both DSB repair pathways by combining olaparib and NU7441 synergistically inhibits HCC growth in both orthotopic HCC mouse and human PDX models. Our work not only establishes versatile tools for in vivo analysis of DNA repair, but also implies an effective combination therapy for HCC.

Author contributions: C.W., H.T., X.W., S.G., Y.J., F.-L.S., and Z.M. designed research; C.W., A.G., B.D., H. Zhang, X.S., Y.C., Z.Q., H. Zhu, J.Y., J.C., Q.H., N.Q., J.X., R.T., and Y.J. performed research; C.W., H.T., A.G., B.D., H. Zhang, X.S., Y.C., Z.Q., H. Zhu, J.Y., J.C., Q.H., J.X., R.T., and Y.J. analyzed data; and C.W., H.T., and Z.M. wrote the paper.

The authors declare no competing interest.

This article is a PNAS Direct Submission. C.H. is a guest editor invited by the Editorial Board.

[1]C.W., H.T., A.G., and B.D. contributed equally to this work.

[2]To whom correspondence may be addressed. Email: ying_jiang@tongji.edu.cn, sfl@tongji.edu.cn, or zhiyong_mao@tongji.edu.cn.

This article contains supporting information online at https://www.pnas.org/lookup/suppl/doi:10.1073/pnas.2002917117/-/DCSupplemental.

First published October 5, 2020.

manner and participates in HR via catalytic activity-independent and -dependent mechanisms (14–17). Nonetheless, it remains to be determined whether and how PARP1 inhibition affects DSB repair in vivo, and whether it can be successfully targeted to treat HR proficient cancers.

Here we compared DSB repair efficiency in HCC with that in adjacent normal tissues, using two knock-in mouse models for in vivo analysis of DSB repair. We found that both the HR and NHEJ pathways were up-regulated in HCC, most likely due to increased expression of PARP1 and DNA-PKcs. We then demonstrated that PARP1 inhibition suppressed HR repair in vivo. Further mechanistic studies showed that PARP1 mediated the recruitment of ALC1 to DSB sites, thereby driving chromatin relaxation and the recruitment of RPA2 and RAD51 to DSB sites. Most dramatically, using both orthotopic HCC mouse models and four HCC patient-derived xenograft (PDX) models, we found that inhibiting PARP1 and DNA-PKcs with olaparib and NU7441 synergistically suppressed the growth of HCC.

Results

Generation of Rosa26HR Reporter Mice. To analyze HR efficiency in mouse liver tissues, we generated Rosa26HR reporter mice with a GFP-based HR reporter integrated into Rosa26 locus (Fig. 1 *A* and *B*). The previously described HR reporter contains two copies of inactivated GFP-Pem1 (18). On the first copy of GFP, a 22-nt deletion together with two I-SceI recognition sites inserted in the first exon of GFP blocks GFP activity, while the second copy of GFP lacks a start codon and the second exon of GFP. When DSBs are induced by I-SceI–mediated DNA digestion, functional GFP can be reconstituted by successful HR. GFP^+ cells can be quantified by immunostaining or FACS to calculate the relative HR efficiency. The targeting HR vector was electroporated into 129S6 mouse embryonic stem (mES) cells, followed by G418 selection. The selected colonies were harvested for DNA extraction, followed by Southern blot analysis with the indicated probe (Fig. 1 *B* and *C*). The mES colonies with the HR reporter integrated into Rosa26 site were then injected into blastocysts. The subsequent chimeric mice were mated with wild-type 129S6 mice. We successfully obtained founder mice, which were genotyped with the indicated primers using PCR (Fig. 1*D*).

To validate the knock-in Rosa26HR reporter mice for the analysis of HR repair efficiency, we transfected +/Rosa26HR mES cells with pCAG-I-SceI vector and analyzed GFP^+ cells by flow cytometry. We observed that 10.1% of mES cells turned GFP^+ (Fig. 1*E*). We further validated the Rosa26HR mES cells by analyzing HR efficiency in cells with two critical HR factors, CtIP and RAD51, depleted. We found that CtIP or RAD51 depletion significantly reduced HR efficiency, by ∼73% and ∼85%, respectively (*SI Appendix*, Fig. S1*A*). In addition, pretreating the Rosa26HR mES cells with mirin, a small molecule inhibiting MRE11A enzymatic activity, led to a 92% reduction in HR efficiency (*SI Appendix*, Fig. S1*B*). These data indicate that the HR reporter in our knock-in mice is functional.

To study NHEJ in vivo, we used the previously reported Rosa26NHEJ reporter mice (Fig. 1*F*) (19), which were genotyped with the indicated primers by PCR (Fig. 1*F*). NHEJ reporter activity was confirmed by introducing I-SceI in vitro into +/Rosa26NHEJ mouse embryonic fibroblasts (MEFs) (*SI Appendix*, Fig. S2 *A* and *B*).

Up-Regulation of HR and NHEJ Efficiency in a Mouse Model of HCC. To analyze DSB repair efficiency in vivo, we capitalized on hydrodynamic tail vein injection as an effective way of introducing exogenous vectors to livers. We injected 30 μg of pEGFP-N1 or pCMV-DsRed2 into the tail vein within a 5-s interval, then killed the mice on day 2 postinjection and dissociated their livers into single-cell suspensions for flow cytometry analysis. Approximately 16.4% GFP^+ and 15.4% $DsRed^+$ hepatocytes were observed (*SI Appendix*, Fig. S3 *A–C*). We then injected different amounts of vectors encoding I-SceI and 15 μg of pCMV-DsRed2 into the tail veins of +/Rosa26NHEJ mice and measured the ratio of GFP^+ cells to $DsRed^+$ cells on day 10 postinjection using an immunofluorescent assay. These experiments revealed a linear relationship between the amount of injected pCMV-I-SceI vector and the $GFP^+/DsRed^+$ ratio (Fig. 2 *A* and *B*), suggesting that this ratio can be used to measure repair efficiency.

To study HCC in vivo, we used a previously reported chemically induced HCC mouse model (20, 21) (Fig. 2*C*). Here 6-wk-old male mice were intraperitoneally (i.p.) injected with diethylnitrosamine (DEN) twice within a 23-d interval, followed by CCl_4 intragastric (i.g.) administration twice weekly starting at day 2 after the first DEN injection, and the oral consumption (p.o.) of 9% alcohol daily starting at day 23 after the first DEN injection. Within 5 mo after the first DEN injection, we observed a decrease in body weight (*SI Appendix*, Fig. S4*A*) and the formation of HCC in ∼95% of the mice (*SI Appendix*, Fig. S4*B*).

To analyze in vivo DSB repair in HCC, we induced HCC in both +/Rosa26HR and +/Rosa26NHEJ mice and then introduced 50 μg of pCMV-I-SceI and 15 μg of pCMV-DsRed2 by hydrodynamic tail veil injection. On day 10 postinjection, HCC and adjacent normal tissues were harvested and processed into frozen sections for immunofluorescence analysis of HR and NHEJ efficiency. We found that the efficiency of both HR and NHEJ as measured by the $GFP^+/DsRed^+$ ratio was significantly increased in HCC tissues relative to adjacent normal tissues, by ∼2.3-fold for HR and 2.5-fold for NHEJ (*SI Appendix*, Fig. S5 *A* and *B*).

Two factors might affect the analysis of DSB repair efficiency, however. The first is the cell cycle phase. HR occurs in S/G2 phase when sister chromatids are available, while NHEJ operates throughout all cell cycle phases (22). The other factor is the transcription level of the reporter gene driven by the Rosa26 promoter. We performed immunostaining experiments with an antibody against Ki67, a widely used marker of proliferation (23), to further quantify the number of proliferating cells (*SI Appendix*, Fig. S5 *C* and *D*). We also performed quantitative PCR to compare the relative in vivo expression level of the reporter gene (*SI Appendix*, Fig. S5 *E* and *F*). We then used the ratio of $GFP^+/DsRed^+$/relative percentage of $Ki67^+$ cells/in vivo transcription level as the measurement of HR and the ratio of $GFP^+/DsRed^+$/in vivo transcription level as the measurement of NHEJ. After comparing the efficiency of HR or NHEJ between HCC tissues and the adjacent normal tissues, we found that the HR and NHEJ pathways were up-regulated in HCC tissues, by 1.6-fold for HR and 2.5-fold for NHEJ (Fig. 2 *D* and *E*).

Elevated Expression of PARP1 and DNA-PKcs in Mouse and Human HCC. Our comparison of protein expression of multiple DSB repair factors in eight pairs of mouse HCC and adjacent normal tissues revealed up-regulated expression of PARP1 and DNA-PKcs in mouse HCC (Fig. 3 *A* and *B*), suggesting that PARP1 and DNA-PKcs play critical roles in the aberrant up-regulation of DSB repair in mouse HCC. Further quantitative PCR experiments revealed highly stimulated mRNA levels of both PARP1 and DNA-PKcs in mouse HCC tissues (*SI Appendix*, Fig. S6*A*), indicating that this up-regulation likely occurs through transcriptional mechanisms.

In contrast, the expression levels of KU70, XRCC4, MRE11A, RAD50, and XRCC3 were down-regulated in mouse HCC (Fig. 3 *A* and *B* and *SI Appendix*, Fig. S6*B*). We propose that the down-regulation of these factors might not affect the efficiency of DSB repair in HCC. Indeed, in murine hepatoma cell line Hepa1-6 that harbors the HR or NHEJ reporter cassette in genomes, a mild knockdown of these proteins did not cause

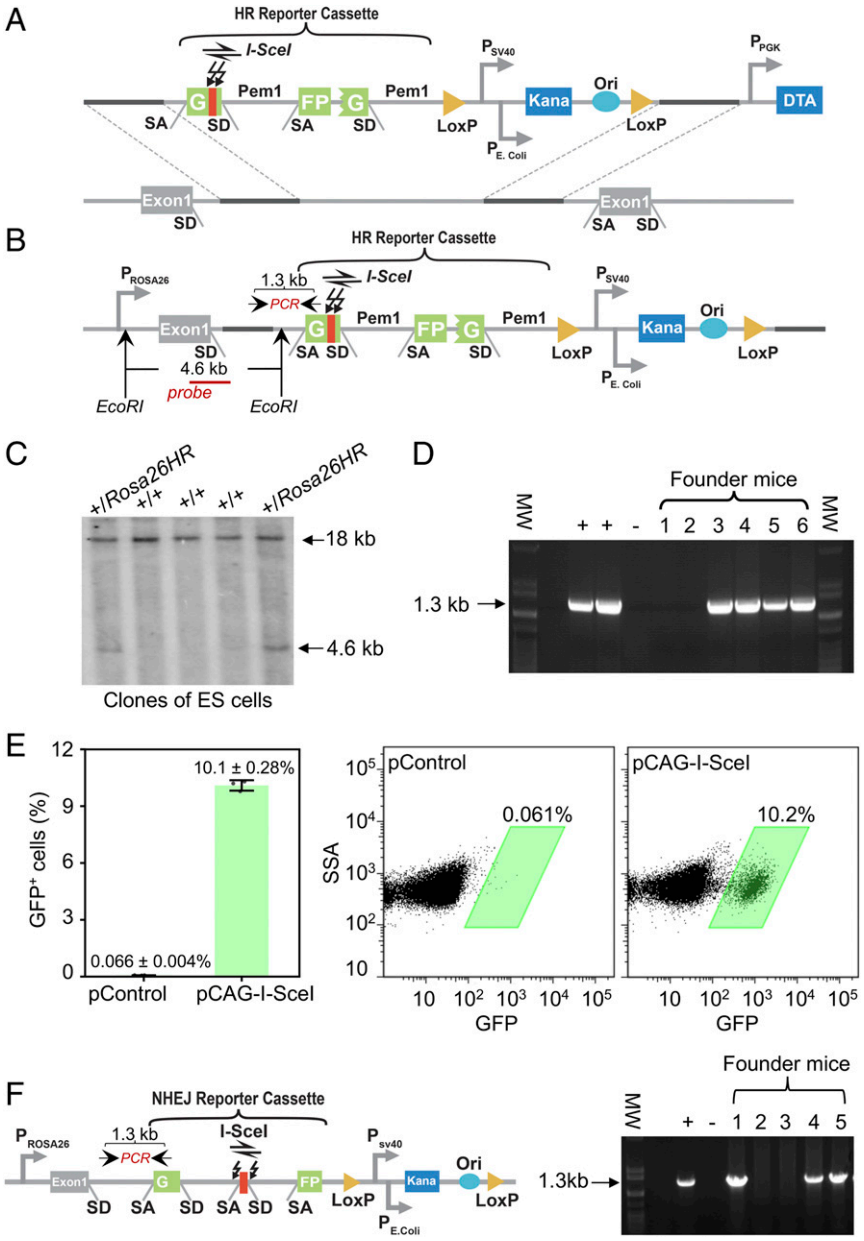

Fig. 1. Knock-in reporter mice for in vivo analysis of HR and NHEJ efficiency. (*A*) The targeting construct containing the HR reporter cassette for integration into the Rosa26 locus. The reporter cassette functions to measure HR efficiency, as described previously (43). (*B*) HR reporter integrated into the Rosa26 site on mouse chromosome 6. (*C*) Southern blot analysis of G418-resistant mES clones. Genomic DNA was extracted from mES clones, followed by EcoRI digestion and Southern blot analysis with the indicated probe. (*D*) PCR analysis of genomic DNA extracted from six founder mice using primers as described previously (19). The two positive controls used genomic DNA extracted from fibroblasts isolated from +/Rosa26NHEJ mice as templates, while no template DNA was added to the negative control PCR. (*E*) FACS analysis of GFP⁺ cells in rapidly proliferating +/Rosa26HR mES cells transfected with 8 μg pCAG-I-SceI vector per 5×10^5 cells. Representative FACS traces for the analysis of GFP⁺ cells resulting from successful HR-directed repair. (*F*) Diagram of the Rosa26NHEJ reporter integrated in the Rosa26 locus. The reporter was described previously (19). PCR analysis of genomic DNA extracted from the founder mice was done using primers as described previously (19). Error bars represent the SD.

significant changes in DSB repair (*SI Appendix*, Fig. S6 *C* and *D*). Since these factors function mainly to facilitate the DNA repair process at DSB sites, we hypothesized that this reduced expression might not affect the amounts of these recruited factors at damage sites. We tested this hypothesis by comparing the recruitment of one of these factors, KU70, in control cells and cells with mild knockdown of KU70 using a chromatin immunoprecipitation (ChIP) assay (16). In control cells, there was a 18.1-fold enrichment of KU70 at I-SceI–generated DSB sites at 2 h after I-SceI transfection, while cells with mild KU70 depletion exhibited a 26.3-fold enrichment of KU70 at the damage sites (*SI Appendix*, Fig. S6*E*). Considering the ∼43% reduction in total KU70 protein level (*SI Appendix*, Fig. S6*D*), the amount of KU70 at the DSB sites was comparable in the control and experimental groups. These data indicate that the decline in global KU70 protein levels might not affect its presence at DSB sites, and thus that the transduction of the subsequent NHEJ signaling cascade is not compromised.

To test whether the up-regulation of PARP1 and DNA-PKcs is conserved between mice and humans, we extracted proteins from 108 sets of human HCC and paired adjacent normal tissues and performed Western blot analysis. Our analysis confirmed that the

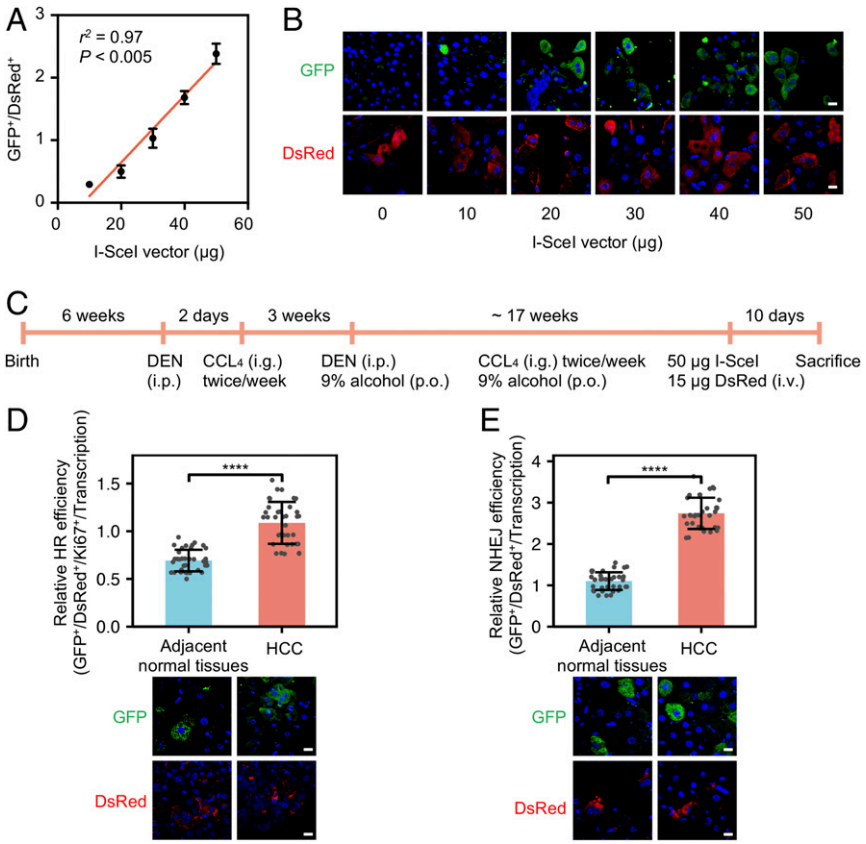

Fig. 2. Both HR and NHEJ are elevated in mouse HCC compared with the adjacent normal tissues. (*A*) Change in the ratio of GFP$^+$ to DsRed$^+$ cells with increasing amounts of pCMV-I-SceI vector introduced into mouse livers via hydrodynamic tail vein injection. On day 10 after injection of I-SceI vector and DsRed vector, mice were killed and their livers were processed into frozen sections. GFP and DsRed immunofluorescence analysis was performed, and the numbers of GFP$^+$ and DsRed$^+$ cells were manually counted (n >3). (*B*) Representative immunostaining pictures of the cells in *A*. (Scale bar: 10 μm.) (*C*) Experimental design of inducing HCC in +/Rosa26HR and +/Rosa26NHEJ reporter mice using the combination of DEN/CCl_4/alcohol treatment. (*D* and *E*) Comparison of HR efficiency measured by the ratio of GFP$^+$/DsRed$^+$ /relative percentage of Ki67$^+$ cells/in vivo transcription level (*D*) and NHEJ efficiency measured by the ratio of GFP$^+$/DsRed$^+$/in vivo transcription level (*E*) among controls, HCC, and adjacent normal tissues in +/Rosa26HR and +/Rosa26NHEJ mice. For each mouse, at least six frozen sections were counted. Representative immunostaining pictures of GFP$^+$ and DsRed$^+$ in mouse livers from controls, HCC, and adjacent normal tissues in +/Rosa26HR or +/Rosa26NHEJ mice are also shown. At least six mice in each group were used. Ki67$^+$ cell number and in vivo transcription levels of the reporter gene are quantified in *SI Appendix*, Fig. S5. Error bars represent the SD. ****P < 0.0001, two-tailed Student's t test. (Scale bar: 10 μm.)

expression levels of PARP1 and DNA-PKcs were up-regulated in human HCC tissues (Fig. 3 *C* and *D*). We then analyzed the mRNA levels of PARP1 and DNA-PKcs using The Cancer Genome Atlas (TCGA) database. In agreement with the mouse HCC experiments, we found that at the mRNA level, both PARP1 and DNA-PKcs were up-regulated in HCC tissues (*SI Appendix*, Fig. S6*F*).

Inhibiting or Depleting Both PARP1 and DNA-PKcs Synergistically Suppresses HCC Cell Survival In Vitro. Since the up-regulation of PARP1 and DNA-PKcs was conserved in mouse and human HCC, we proposed that these two factors are particularly critical for the survival of HCC. Thus, we examined whether inhibiting PARP1 with olaparib and DNA-PKcs with NU7441 could affect the survival of Hep3B and Huh7. We found that inhibiting both factors significantly reduced the survival of Hep3B (2 μM olaparib:2 μM NU7441:both = 5.1%:14.8%:67.8%) and Huh7 (2 μM olaparib:2 μM NU7441:both = 10.7%:30.8%:75.2%) (Fig. 4*A*). Calculation of the combination index of the combination therapy revealed that olaparib and NU7441 synergistically suppressed HCC survival (Fig. 4*B* and *SI Appendix*, Fig. S7). These results indicate that at least one factor, either PARP1 or DNA-PKcs, with full catalytic activity is required for the survival of HCC cells.

Since PARP1 inhibitors were reported to trap PARP1 at DNA damage sites to induce cytotoxicity (24), it is possible that the failure to remove PARP1 from DSB sites sensitizes HCC cells to NU7441. We next examined whether depleting both factors affected the survival of HCC cells. We found that moderate depletion of both PARP1 and DNA-PKcs mildly but synergistically inhibited cell survival in Hep3B cells by 48.9%, while a robust knockdown of both PARP1 and DNA-PKcs led to a more drastic reduction in cell survival in Hep3B cells, by ~81% (Fig. 4 *C* and *D* and *SI Appendix*, Fig. S8), indicating that the increased cytotoxicity is not caused by the trapping of PARP1 at DNA damage sites.

Similarly, in Huh7 cells, depletion of both factors synergistically inhibited cell survival (shPARP1:shDNA-PKcs:both = 8.1%:33%:86.4%) (*SI Appendix*, Fig. S9 *A*–*C*). Moreover, we established Huh7 xenografts in nude mice by inoculating Huh7 cells with PARP1 or/and DNA-PKcs depleted. In agreement with the in vitro results, depleting both PARP1 and DNA-PKcs synergistically inhibited the growth of Huh7 xenografts (*SI Appendix*, Fig. S9 *D* and *E*).

Consequently, inhibiting both factors led to an increase in the number of γH2AX$^+$ Hep3B cells (control:olaparib:NU7441:olaparib + NU7441 = 5.2%:13.0%:15.1%:50.5%) (Fig. 4*E*), and high rates of apoptosis as assayed by caspase-3$^+$ cells (control:olaparib:NU7441:olaparib + NU7441 = 14.6%:19.9%:32.4%:82.7%) (Fig. 4*F*). Western blot

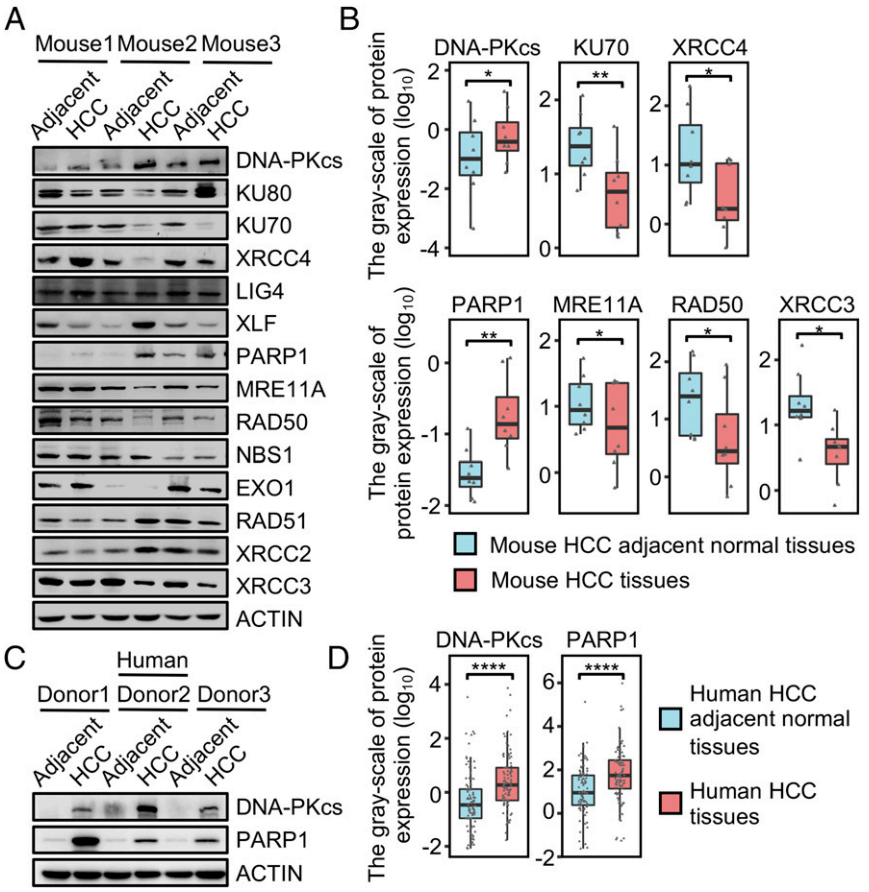

Fig. 3. Expression levels of PARP1 and DNA-PKcs are elevated in both mouse and human HCC compared with adjacent normal tissues. (*A*) Eight pairs of HCC and adjacent normal tissues were harvested from DEN/CCl_4/alcohol-treated mice, followed by protein extraction and Western blot analysis with indicated antibodies. Representative pictures show three pairs of HCC and adjacent normal tissues. (*B*) Comparison of the expression levels of DSB repair factors between mouse HCC and adjacent normal tissues ($n = 8$). (*C*) One hundred and eight sets of human HCC and paired adjacent normal tissues were prepared during surgery, followed by protein extraction and Western blot analysis with indicated antibodies. Representative pictures show three pairs of HCC and adjacent normal tissues. (*D*) Comparison of the expression levels of PARP1 and DNA-PKcs in 108 pairs of human HCC and adjacent normal tissues. The expression of DSB repair factors in mouse or human tissues was quantified using ImageJ software. Error bars represent the SD. $^{*}P < 0.05$; $^{**}P < 0.01$; $^{****}P < 0.0001$, two-tailed paired Student's *t* test.

analysis confirmed the high levels of γH2AX and caspase-3 in Hep3B cells in the presence of both inhibitors (*SI Appendix*, Fig. S10 *A* and *B*).

PAR-Mediated Recruitment of ALC1 to DSB Sites Relaxes Chromatin and Promotes HR in HCC. Since PARP1 participates in alt-NHEJ in an enzymatic activity-dependent manner (14) and DNA-PKcs is a well-documented factor involved in c-NHEJ, we proposed that in HCC tissues, inhibiting PARP1 enzymatic activity with olaparib impairs HR repair. To examine whether and how olaparib and NU7441 affect DSB repair in HCC tissues, we administered olaparib or/and NU7441 to +/Rosa26HR or +/Rosa26NHEJ mice with induced HCC BY i.p. injection for 15 consecutive days. On day 5 after drug administration, plasmids encoding I-SceI and DsRed were delivered to livers via hydrodynamic tail vein injection. On day 15 after drug administration, the mice were killed for analysis of DSB repair efficiency. Immunostaining analysis revealed that both olaparib and olaparib/NU7441 significantly suppressed HR efficiency measured by the ratio of $GFP^+/DsRed^+$/relative percentage of $Ki67^+$ cells/in vivo transcription level by ∼81% and 57% or HR efficiency measured by the ratio of $GFP^+/DsRed^+$ ratio by ∼77% and 57%, while NU7441 treatment stimulated HR efficiency measured by the ratio of $GFP^+/DsRed^+$/relative percentage of $Ki67^+$ cells/in vivo transcription level by ∼56% and HR efficiency measured by the ratio of $GFP^+/DsRed^+$ by 56% in HCC (Fig. 5*A* and *SI Appendix*, Fig. S11 *A* and *B* and Fig. S12 *A*–*C*). In adjacent normal tissues, olaparib or olaparib/NU7441 treatment had a very mild effect on HR, while NU7441 forced normal hepatocytes in the adjacent normal tissues to choose HR, consistent with the trend seen in HCC tissues (Fig. 5*A* and *SI Appendix*, Fig. S11 *A* and *B* and Fig. S12 *A*–*C*). Furthermore, we found that, in agreement with the known function of PARP1 in alt-NHEJ, inhibiting PARP1 by olaparib mildly suppressed NHEJ efficiency measured by the ratio of $GFP^+/DsRed^+$/in vivo transcription level by 28% or NHEJ efficiency measured by the ratio of $GFP^+/DsRed^+$ by 27% in HCC (Fig. 5*A* and *SI Appendix*, Fig. S11 *C* and *D* and Fig. S12*D*), while NU7441 and NU7441/olaparib treatment inhibited NHEJ efficiency measured by the ratio of $GFP^+/DsRed^+$/in vivo transcription level by ∼33% and ∼61% and NHEJ efficiency measured by the ratio of $GFP^+/DsRed^+$ by ∼38% and 62%. In adjacent normal tissues, all treatments reduced NHEJ efficiency measured by the ratio of $GFP^+/DsRed^+$/in vivo transcription level by ∼42 to 54% and NHEJ efficiency measured by the ratio of $GFP^+/DsRed^+$ by ∼45 to 55% (Fig. 5*A* and *SI Appendix*, Fig. S11 *C* and *D* and Fig. S12*D*).

To understand how PARP1 participates in HR in HCC, we performed immunoprecipitation (IP) experiments with a PARP1

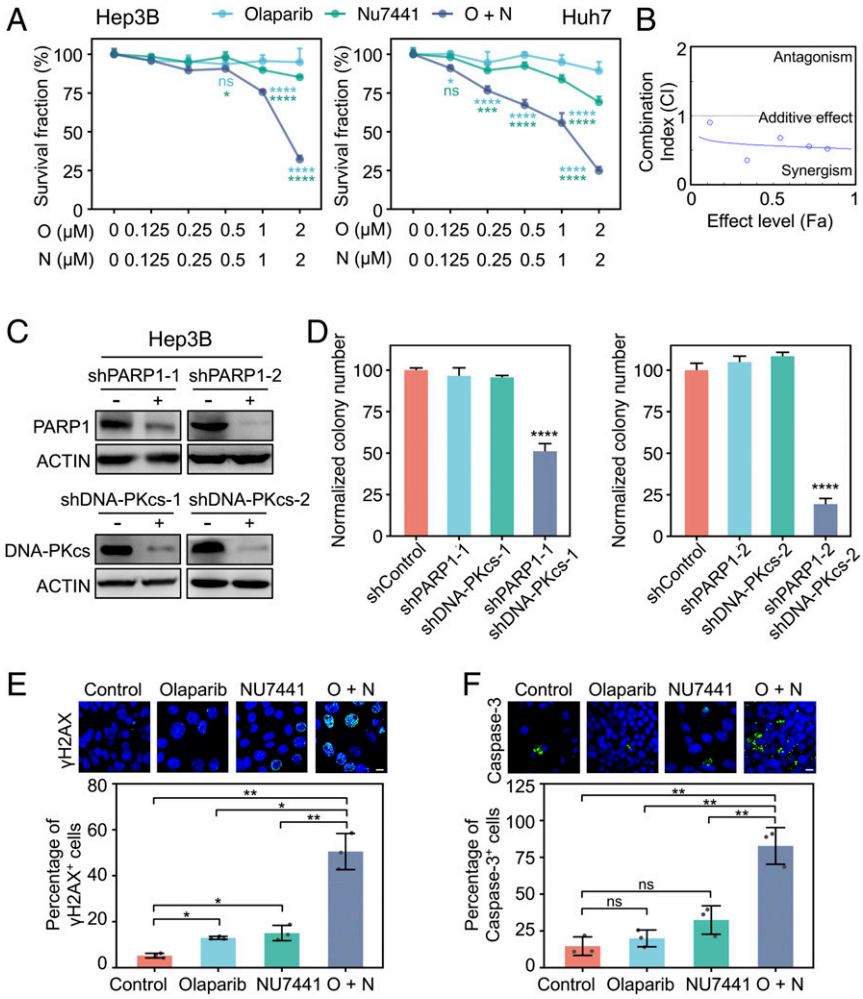

Fig. 4. Inhibiting or knocking down both PARP1 and DNA-PKcs synergistically suppresses HCC cell survival. (*A*) Clonogenic assay analyzing the survival rates of Hep3B and Huh7 cells in the presence of olaparib or/and NU7441 with increasing concentrations ($n = 3$ for each group). (*B*) Isobologram analysis of olaparib and NU7441 combination therapy using CompuSyn. A combination index <1.0 indicates a synergistic effect. (*C*) Western blot analysis of PARP1 and DNA-PKcs expression levels in cells infected with lentivirus bearing shPARP1 or shDNA-PKcs in Hep3B cells. (*D*) Clonogenic assay analyzing survival rates of Hep3B cells with PARP1 or/and DNA-PKcs depleted ($n = 3$ for each group). (*E*) Immunofluorescence analysis with an antibody against γH2AX in Hep3B cells treated with olaparib or/and NU7441. (*F*) Immunofluorescence analysis with an antibody against caspase-3 in Hep3B cells treated with olaparib or/and NU7441. Error bars represent the SD. *$P < 0.05$; **$P < 0.01$; ***$P < 0.001$; ****$P < 0.0001$, two-tailed Student's *t* test. ns, not significant. (Scale bar: 10 μm.)

antibody in a pair of human HCC samples and associated adjacent normal tissue, followed by mass spectrometry analysis. We did not identify any conventional HR factors interacting with PARP1 in HCC (Fig. 5*B* and *SI Appendix*, Fig. S13); instead, we found that ALC1, which is recruited to DNA damage sites and plays a role in nucleotide excision repair in a PAR-dependent manner (25–27), interacted with PARP1 in the HCC tissue (Fig. 5*B*). Co-IP followed by Western blot analysis confirmed that more ALC1 interacted with PARP1 in the HCC (Fig. 5*C*). Moreover, our co-IP experiments with an antibody against PAR also revealed that PARP1 might interact with ALC1 through its PAR chain in HCC (Fig. 5*D*). In addition, we performed co-IP experiments in cells overexpressing PARP1 wild-type (WT) or PARP1 enzymatically inactive mutant (E988K) and found that the catalytically dead mutant PARP1 E988K did not interact with ALC1 (Fig. 5*E*), suggesting that the interaction between PARP1 and ALC1 is mediated by the PAR chain.

To further elucidate the regulatory mechanisms of HR suppression by olaparib, we chromosomally integrated our HR reporter into Hep3B cells. Pretreating Hep3B-HR cells with 1 μM olaparib significantly reduced HR efficiency, by ~45% (Fig. 5*F*). We ruled out the possibility that olaparib inhibits HR through arresting cells in G1, because we did not observe significant changes in either cell cycle distribution or EdU incorporation rates in Hep3B cells treated with 1 μM olaparib (*SI Appendix*, Fig. S14 *A* and *B*).

We then hypothesized that PARylated PARP1 mediates the recruitment of ALC1 to DNA damage sites and relaxes chromatins, thereby promoting HR repair. ChIP experiments demonstrated that ALC1 was recruited to I-SceI–induced DSB sites, and that olaparib suppressed the recruitment (Fig. 5*G*). In addition, depletion of ALC1 reduced the HR efficiency in Hep3B cells by ~41%, while supplementation of olaparib to ALC1-depleted cells did not cause any further reduction in HR repair (Fig. 5*H* and *SI Appendix*, Fig. S14*C*), suggesting that ALC1 and PARP1 function in the same pathway.

We also examined the change in nucleosome density on the induction of DSBs in Hep3B cells with ALC1 knockdown or olaparib treatment, as described previously (28). We found that either ALC1 depletion or PARP1 inhibition impaired the capacity for reducing nucleosome density at DSB sites, while treatment of ALC1-depleted cells with olaparib did not have any

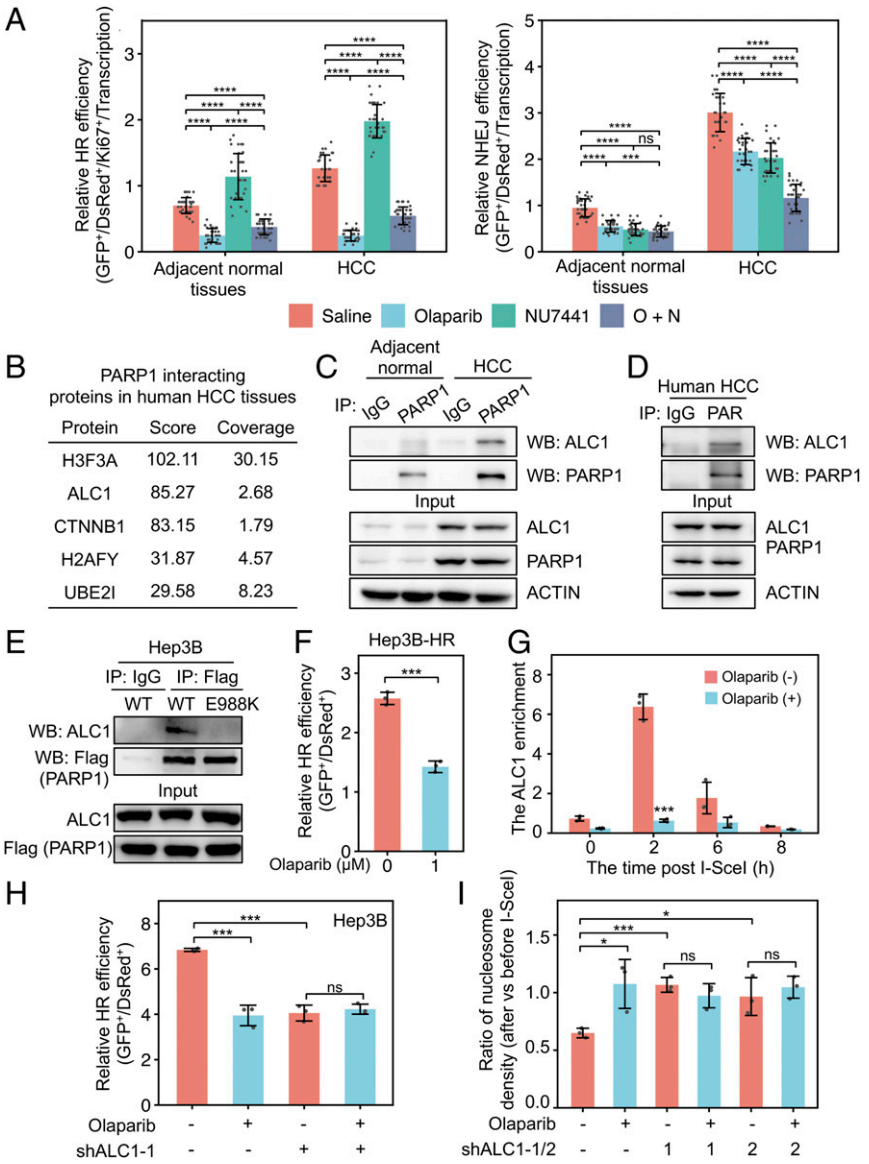

Fig. 5. Inhibiting PARP1 by olaparib reduces HR by suppressing the ALC1-mediated clearance of nucleosomes at DNA damage sites. (*A*) Analysis of HR efficiency measured by the ratio of GFP$^+$/DsRed$^+$/relative percentage of Ki67$^+$ cells/in vivo transcription level and NHEJ efficiency measured by the ratio of GFP$^+$/DsRed$^+$/in vivo transcription level in mouse HCC and adjacent normal tissues with olaparib or/and NU7441 injected i.p. The +/Rosa26HR or +/Rosa26NHEJ mice with DEN/CCl_4/alcohol-induced HCC were pretreated with olaparib or/and NU7441 for 15 consecutive days before being dosed with 50 μg of pCMV-I-SceI vector and 15 μg of pCMV-DsRed2 via hydrodynamic tail vein injection, followed by drug treatment for another 15 consecutive days before the mice were killed. The induction of HCC was similar to the method described in Fig. 2*C*, except that in this experiment, the CCl_4 (i.g.) twice weekly and 9% alcohol (p.o.) treatment was extended from 17 wk (Fig. 2*C*) to 21 wk to promote the efficiency of orthotopic HCC development. The analysis of repair efficiency is the same as that described in Fig. 2 *D* and *E*. The quantification of Ki67$^+$ cell number and transcription level of the reporter gene are shown in *SI Appendix*, Fig. S12. For each group, at least six mice were analyzed. (*B*) ALC1 interacts with PARP1 or PAR in a human HCC tissue. Co-IP with PARP1 antibody followed by mass spectrometry analysis identified ALC1 as among the factors potentially interacting with PARP1 in human HCC. (*C* and *D*) Co-IP followed by Western blot analysis confirmed the interaction between ALC1 and PARP1 (*C*) or PAR (*D*) in human HCC tissue. (*E*) PARP1 WT, but not the enzymatically dead mutant PARP1 E988K, interacts with ALC1. A vector encoding PARP1 WT-Flag or E988K-Flag mutant was transfected to Hep3B cells, followed by co-IP experiments with an antibody recognizing Flag and then Western blot analysis with an ALC1 antibody. (*F*) Changes in HR efficiency in the presence of olaparib at 1 μM in Hep3B-HR cells containing chromosomally integrated HR reporter ($n = 3$). (*G*) Olaparib treatment abrogated the recruitment of ALC1 to I-SceI–generated site-specific DSBs ($n = 3$). (*H*) Depletion of ALC1 did not have any additional suppressive effect on HR in Hep3B-HR treated with olaparib at 1 μM ($n = 3$). (*I*) Supplementing olaparib to ALC1 knockdown cells did not have any further negative effect on nucleosome clearance at DSB sites in Hep3B-HR cells. The calculation of the nucleosome density at DNA damage sites was calculated as described previously (17). Error bars represent the SD. *$P < 0.05$; ***$P < 0.001$; ****$P < 0.0001$, two-tailed Student's *t* test. ns, not significant.

additional effects on nucleosome density (Fig. 5*I*), suggesting that chromatin relaxation mediated by ALC1 at DSB sites relies on PARP1 enzymatic activity. Subsequent immunostaining experiments showed that olaparib did not impair the recruitment of γH2AX but significantly inhibited the recruitment of RPA2 (by 68.5%) and RAD51 (by 63.0%) to DNA damage sites in Hep3B cells (*SI Appendix*, Fig. S14 *D–F*), confirming that PARP1 indeed operates in HR repair between the steps of DNA damage response and end resection, likely at the step of chromatin relaxation.

Mouse HCC Is Sensitive to the Combination of olaparib and NU7441. Since the combination of olaparib and NU7441 blocked both HR and the two sub-NHEJ pathways, destabilizing genomes and promoting apoptosis in HCC cells, we next assessed whether this combination could suppress orthotopic HCC growth in mouse models. HCC was induced in male C57BL/6 mice as described above (Fig. 2*C*), followed by a 28-d consecutive treatment with i.p. injection of saline or olaparib or/and NU7441. The mice were then killed, and the endpoint tumor volumes were quantified. We found that the combination therapy greatly suppressed tumor growth (Fig. 6*A* and *SI Appendix*, Fig. S15). Analysis of the endpoint tumor growth inhibition (TGI) rate showed that combination treatment with olaparib and NU7441 led to a 75.6% increase in the TGI, compared with a 1.9% decrease with single-agent olaparib and a 7.9% increase with single-agent NU7441 treatment (Fig. 6*B*), indicating that the combination of the two drugs holds the potential for HCC therapy. We also observed a significant decline in relative aspartate transaminase and alanine transaminase levels in the group of induced HCC mice that received combination therapy (*SI Appendix*, Fig. S16), indicating improved liver functions in the combination therapy group.

In addition, the analysis of hepatotoxicity, nephrotoxicity, and cardiotoxicity in healthy mice receiving combination therapy indicated that the combination therapy had no significant toxicity in the liver, kidney, and heart (*SI Appendix*, Fig. S17). Moreover, the combination therapy had a very mild effect on body weight (*SI Appendix*, Fig. S18). Taken together, these results suggest a low toxicity of this drug combination.

Combination Treatment with Olaparib and NU7441 Is a Potential Therapy for Human HCC. Our further assessment using the TCGA data portal revealed that low expression levels of both PARP1 and DNA-PKcs predicted better survival than that in patients with

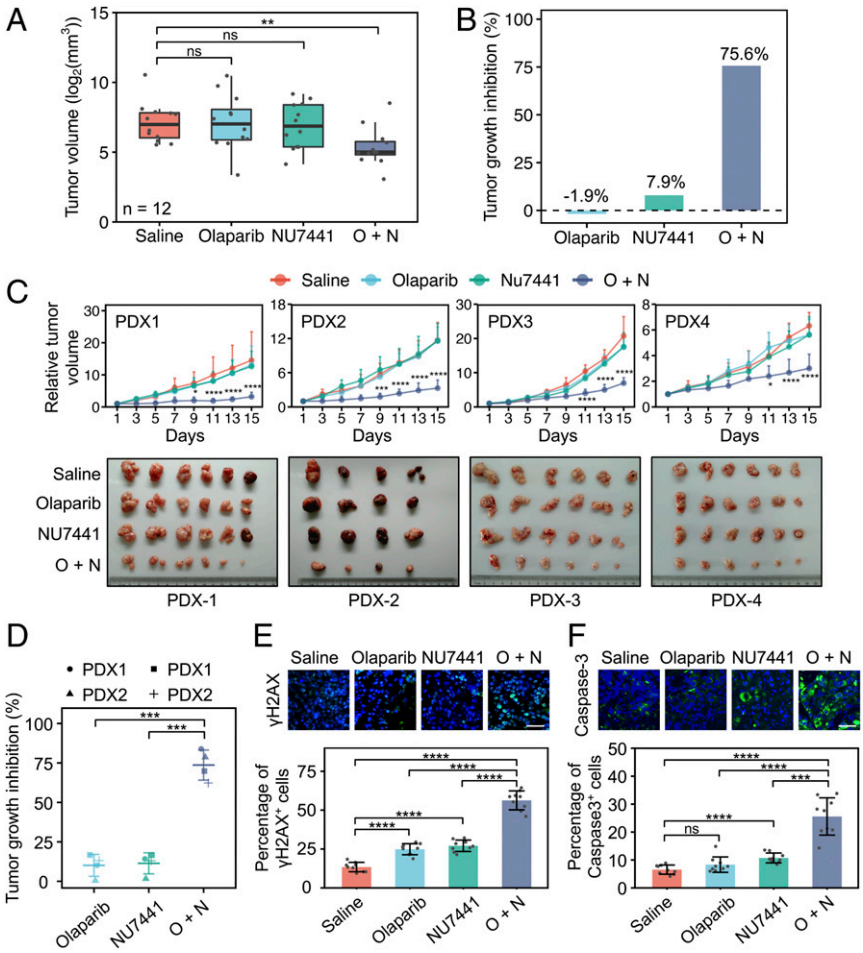

Fig. 6. Combination therapy with olaparib and NU7441 synergistically suppresses the growth of mouse HCC induced by DEN/CCl_4/alcohol, and four human HCC PDX models growing in nude mice. (*A*) Comparison of the calculated volumes of mouse HCC between groups receiving different treatments. Mouse HCC induced by DEN/CCl_4/alcohol was sensitive to the combined treatment with olaparib and NU7441. At least 12 mice in each group were analyzed. (*B*) Comparison of mouse HCC TGI rate between the control group and drug-treated groups. $[(MTVcontrol_{tn} - MTVtreated_{tn})/(MTVcontrol_{tn} - MTVcontrol_{t0})] \times 100$ was used for calculating TGI. MTV, mean tumor volume; t0, start of the treatment; tn, end of the treatment. (*C*) Tumor volume measurement of four PDXs carried by nude mice in response to different treatments. Nude mice carrying four human HCC PDX models were treated with saline, olaparib and/or NU7441 for 15 consecutive days. Tumor volumes were measured every other day. At least six nude mice carrying human PDX were measured for each group. Representative pictures of human HCC PDX1–4 isolated from nude mice receiving different drug therapies are also shown. Statistical analysis was performed using two-way ANOVA followed by Turkey's multiple comparison test. (*D*) Comparison of human HCC TGI rate among different therapeutic approaches. (*E*) Representative immunostaining pictures and quantification of γH2AX foci-positive cells in sections of PDX1 receiving different treatments. The numbers of $\gamma H2AX^+$ cells (>10 foci) in nine noncontinuous regions of PDX1 sections were counted. (*F*) Representative immunostaining pictures and quantification of caspase-3^+ cells in PDX1 sections treated with different drugs. The numbers of caspase-3^+ cells in nine noncontinuous regions of PDX1 sections were counted ($n = 3$). In *E* and *F*, error bars represent the SD. $^*P < 0.05$; $^{**}P < 0.01$; $^{***}P < 0.001$; $^{****}P < 0.0001$, two-tailed Student's *t* test. ns, not significant. (Scale bar: 50 μm.)

high expression levels of the two factors ($P = 0.01$) (*SI Appendix*, Fig. S19), indicating that simultaneous inhibition of PARP1 and DNA-PKcs is a potentially effective approach to treating HCC. To determine whether the combination of the two drugs can be applied in the clinic, we used human HCC PDX models, which faithfully resemble the original characteristics of primary tumors, such as the heterogeneity and histological structures. Among the four HCC PDX models, two were HBV-positive (PDX1 and PDX3) and the other two were HBV-negative (PDX2 and PDX4) (*SI Appendix*, Fig. S20).

Saline, olaparib, NU7441, or the olaparib-NU7441 combination were i.p. injected in PDX-bearing mice for 15 consecutive days. We found that the four PDXs responded well to the combination treatment, while single drug treatments had very mild suppressive effects on HCC growth (Fig. 6 *C* and *D*), consistent with orthotopic HCC data (Fig. 6 *A* and *B*). On day 15 posttreatment, we found that the combination of olaparib and NU7441 had inhibited the growth of PDX1–4 by 83.9%, 78.6%, 68.9% and 62.3%, respectively (Fig. 6 *C* and *D*), which was higher than the standard endpoint TGI rate of 60.0% (29). In contrast, the average TGI rate was only 10.1% for olaparib and 11.4% for NU7441 (Fig. 6*D*). These data strongly indicate that the combination of olaparib and NU7441 has synergistic effects on HCC growth suppression.

Immunostaining experiments with antibodies against γH2AX and caspase-3 in PDX1 tumor samples revealed that only the combination therapy resulted in the accumulation of $\gamma H2AX^+$ cells (saline:olaparib:NU7441:olaparib + NU7441 = 13.4%:24.9%:27.1%:56.3%) (Fig. 6*E*) and a significant increase in caspase-3^+ cells (saline: olaparib:NU7441:olaparib + NU7441 = 6.6%:8.3%:10.7%:25.6%) (Fig. 6*F*). Thus, the combination of olaparib and NU7441 is an effective therapy for HCC in PDX models by inhibiting DSB repair.

Discussion

Understanding the differences in DSB repair capacity between HCC and normal liver tissue would provide valuable insight into developing DNA repair-targeted cancer therapy. Although it is feasible to compare the change in DSB repair efficiency between tumor and normal cells (30), establishing and optimizing the growth conditions for culturing primary HCC and normal hepatocyte cells is technically challenging. Moreover, whether the conclusions drawn from in vitro experiments faithfully reflect the situation in vivo remains largely unknown. Our present work overcame these major obstacles by establishing in vivo assays for measuring HR and NHEJ in livers using two knock-in reporter mouse models.

Similar to other types of cancers, HCC is associated with mutations in a number of genes (31). The Rosa26HR and Rosa26NHEJ knock-in reporter mice provide versatile tools for understanding whether and how these frequently mutated genes impact HCC tumorigenesis and tumor maintenance, thus providing hints for HCC prevention and therapy in different genetic backgrounds. Previous reports have demonstrated that crossing of pCMV-rtTA transgenic mice, pTRE-I-SceI transgenic mice, and DR-GFP reporter mice enables the assessment of HR efficiency in such organs as the mammary glands and intestines (32–34). Combining the pCMV-rtTA transgenic mice and pTRE-I-SceI transgenic mice with Rosa26HR and Rosa26NHEJ mice could potentially extend our knowledge of DNA repair change to other types of tumors, as well as in different biological contexts, such as aging or other types of diseases.

Using the Rosa26HR and Rosa26NHEJ knock-in reporter mice together with clinical samples, we have demonstrated that the up-regulated HR and NHEJ pathways contribute to HCC tumor maintenance. The increase in HR efficiency is not surprising, as the rapid proliferation of cancer cells causes high replication stress, which can be relieved by HR (10). Why is the NHEJ pathway, which is commonly believed to be associated with radioresistance and chemoresistance (35), also up-regulated in HCC? We hypothesized that in HCC, possibly more spontaneous DSBs are induced by elevated levels of reactive oxygen species (ROS) (9). The DSBs induced by ROS could occur at any chromatin region and can be repaired by both HR and NHEJ. Therefore, an enhanced NHEJ pathway may also contribute to HCC maintenance. Nevertheless, although more DSBs are observed in HCC compared with adjacent normal tissues (36), whether they are generated mainly by ROS remains to be determined.

Of note, we also observed no correlation between mRNA level and protein abundance in several genes, including MRE11A, RAD50, and XRCC3. How to reconcile this discrepancy? In many scenarios, mRNA level cannot be used to predict the protein level (37). We propose that in HCCs, the mRNA transcripts of these genes might not be efficiently translated into proteins, or the proteins might be more unstable.

Although HCC takes advantage of DSB repair pathways for its survival, we also demonstrated that the elevated HR and NHEJ represent an Achilles' heel for this cancer. Unfortunately, although the development of small molecules targeting classical factors involved in DSB repair for cancer therapy has long received much attention (38), none of them has successfully completed clinical trials. Serendipitously, our mechanistic studies found that PARP1, whose inhibitors olaparib, rucaparib, and niraparib have been approved by the Food and Drug Administration (39), was up-regulated at the protein level and participated in HR by altering the chromatin context through the recruitment of ALC1 to DSB sites. However, since PARP1 is involved in both single-strand break repair and HR, one would expect that inhibiting PARP1 with olaparib alone would lead to the accumulation of DSBs generated by collapsed DNA replication forks, resulting in the "BRCAness" phenotype, which we did not observe in this study. This surprising finding can be reconciled by that fact that the HR-directed repair of DSBs generated by collapsed replication forks probably occurs in a PARP1-independent manner as the PARP1-mediated chromatin relaxation at DNA damage sites is not likely necessary at replication forks where nucleosomes are dissembled (40).

The NHEJ pathway is active throughout the entire cell cycle, including S phase when HR occurs (22). Although monotherapy with olaparib is able to suppress both HR and alt-NHEJ, the remaining active c-NHEJ is apparently sufficient to maintain HCC growth in vitro and in vivo. Only the combination of olaparib with NU7441 to block c-NHEJ by inhibiting the enzymatic activity of DNA-PKcs, which is significantly up-regulated in both mouse and human HCC, can drastically reduce HCC growth rate. Although previous reports indicated that the pharmacokinetic properties of NU7441, such as insolubility in water and rapid in vivo metabolization, might hamper its potential clinical applications (41), our promising results at least demonstrate that combining DNA-PKcs inhibitors with PARP1 inhibitors holds the potential to treat HCC. Fortunately, several other DNA-PKcs inhibitors with better pharmacokinetic properties are under investigation in phase I clinical trials (42). Whether combining the latest generation of DNA-PKcs inhibitors with PARP1 inhibitors will yield better responses to HCC requires further investigation, as does whether combining radiotherapy to generate some amounts of DSBs with the combination therapy will yield better responses.

In summary, our work has established a method of in vivo analysis of HR and NHEJ efficiency in livers using our Rosa26HR and Rosa26NHEJ knock-in reporter mice. Based on the reporter mice, we demonstrated that in HCC, both HR and NHEJ were up-regulated to maintain HCC growth. Our mechanistic studies indicate that in HCC, high expression of PARP1 and DNA-PKcs

contributes to the increased HR and NHEJ efficiency. We also elucidated the role of the PARP1-ALC1 axis in regulating HR repair. Most importantly, we have demonstrated that the combination therapy of olaparib and NU7441 is an effective method for treating HCC (*SI Appendix*, Fig. S21).

Materials and Methods

Animal Use and Generation of the Rosa26HR Knock-In Reporter Mouse Line. All animal maintenance and experiments were performed in accordance with the Tongji University of Health Guide for the Care and Use of Laboratory Animals and were approved by the Biological Research Ethics Committee of Tongji University. Mice were housed under a 12-h light/dark cycle under pathogen-free conditions at 22 ± 2 °C and given free access to standard mouse chow and tap water.

The HR targeting vector was generated based on a Rosa26NHEJ targeting vector (19) and the previously described HR reporter cassette (18, 43). The resulting targeting vector was then electroporated into 129S6 mES cells, followed by G418 selection. The G418-resistant colonies were then harvested for DNA extraction, followed by Southern blot analysis after EcoRI digestion.

Generation of PDX Models and Drug Treatment In Vivo. All human HCC and adjacent normal tissues were obtained from Shanghai Eastern Hepatobiliary Surgery Hospital upon written informed consent. All experiments with human material were conducted with the ethical approval from the Ethics Committees of Tongji University (2018yxy02) and Shanghai Eastern Hepatobiliary Surgery Hospital (EHBHKY2017-K-004). Human HCC tissues were cut into 1-mm^3 sections and transplanted into nude mice to create PDX models. Successfully engrafted tumors were passaged once before being transplanted into 30 nude mice. When tumor size reached 50 mm^3, the nude mice were randomized into four groups that received treatment with saline, olaparib (50 mg/kg/d), NU7441 (4 mg/kg/d), or both drugs (olaparib and NU7441) through i.p. injections. The daily treatment lasted 15 consecutive days, with tumor size measured using calipers every 2 d. Tumor volume was calculated as $width^2 \times length/2$.

Data Availability. All study data are included in the main text and *SI Appendix*.

ACKNOWLEDGMENTS. We thank Drs. Michael Van Meter and Shuning He for critically reading the manuscript; and Drs. Vera Gorbunova and Andrei Seluanov (University of Rochester) for kindly providing the Rosa26NHEJ mice. This work was supported by grants from Chinese National Program on Key Basic Research Project (2017YFA010330 and 2018YFC2000100), the National Science Foundation of China (31871438, 81972457, and 31871446), the Fundamental Research Funds for the Central Universities, Program of Shanghai Academic Research Leader (19XD1403000), the Shuguang Program of the Shanghai Education Development Foundation and Shanghai Municipal Education Commission (19SG18), the Shanghai Municipal Health Commission (2017ZZ02015), and the Hunan Provincial Science and Technology Department (2019JJ40482).

1. L. A. Torre *et al*., Global cancer statistics, 2012. *CA Cancer J. Clin.* **65**, 87–108 (2015).
2. S. F. Altekruse, K. A. McGlynn, M. E. Reichman, Hepatocellular carcinoma incidence, mortality, and survival trends in the United States from 1975 to 2005. *J. Clin. Oncol.* **27**, 1485–1491 (2009).
3. M. Jasin, R. Rothstein, Repair of strand breaks by homologous recombination. *Cold Spring Harb. Perspect. Biol.* **5**, a012740 (2013).
4. K. K. Chiruvella, Z. Liang, T. E. Wilson, Repair of double-strand breaks by end joining. *Cold Spring Harb. Perspect. Biol.* **5**, a012757 (2013).
5. A. J. Pierce, M. Jasin, NHEJ deficiency and disease. *Mol. Cell* **8**, 1160–1161 (2001).
6. F. Dietlein, L. Thelen, H. C. Reinhardt, Cancer-specific defects in DNA repair pathways as targets for personalized therapeutic approaches. *Trends Genet.* **30**, 326–339 (2014).
7. N. C. Teoh *et al*., Defective DNA strand break repair causes chromosomal instability and accelerates liver carcinogenesis in mice. *Hepatology* **47**, 2078–2088 (2008).
8. S. F. Yang *et al*., Involvement of DNA damage response pathways in hepatocellular carcinoma. *BioMed Res. Int.* **2014**, 153867 (2014).
9. G. Y. Liou, P. Storz, Reactive oxygen species in cancer. *Free Radic. Res.* **44**, 479–496 (2010).
10. H. Gaillard, T. García-Muse, A. Aguilera, Replication stress and cancer. *Nat. Rev. Cancer* **15**, 276–289 (2015).
11. C. J. Lord, A. N. Tutt, A. Ashworth, Synthetic lethality and cancer therapy: Lessons learned from the development of PARP inhibitors. *Annu. Rev. Med.* **66**, 455–470 (2015).
12. J. S. Brown, S. B. Kaye, T. A. Yap, PARP inhibitors: The race is on. *Br. J. Cancer* **114**, 713–715 (2016).
13. A. Dréan, C. J. Lord, A. Ashworth, PARP inhibitor combination therapy. *Crit. Rev. Oncol. Hematol.* **108**, 73–85 (2016).
14. M. Wang *et al*., PARP-1 and Ku compete for repair of DNA double-strand breaks by distinct NHEJ pathways. *Nucleic Acids Res.* **34**, 6170–6182 (2006).
15. S. Xie *et al*., Timeless interacts with PARP-1 to promote homologous recombination repair. *Mol. Cell* **60**, 163–176 (2015).Correction in: *Mol. Cell.* **61**, 181 (2016).
16. H. Liu *et al*., Nuclear cGAS suppresses DNA repair and promotes tumorigenesis. *Nature* **563**, 131–136 (2018).
17. Y. Chen *et al*., A PARP1-BRG1-SIRT1 axis promotes HR repair by reducing nucleosome density at DNA damage sites. *Nucleic Acids Res.* **47**, 8563–8580 (2019).
18. Z. Mao *et al*., SIRT6 promotes DNA repair under stress by activating PARP1. *Science* **332**, 1443–1446 (2011).
19. A. Vaidya *et al*., Knock-in reporter mice demonstrate that DNA repair by non-homologous end joining declines with age. *PLoS Genet.* **10**, e1004511 (2014).
20. P. Newell, A. Villanueva, S. L. Friedman, K. Koike, J. M. Llovet, Experimental models of hepatocellular carcinoma. *J. Hepatol.* **48**, 858–879 (2008).
21. L. Bakiri, E. F. Wagner, Mouse models for liver cancer. *Mol. Oncol.* **7**, 206–223 (2013).
22. Z. Mao, M. Bozzella, A. Seluanov, V. Gorbunova, DNA repair by nonhomologous end joining and homologous recombination during cell cycle in human cells. *Cell Cycle* **7**, 2902–2906 (2008).
23. T. Scholzen, J. Gerdes, The Ki-67 protein: From the known and the unknown. *J. Cell. Physiol.* **182**, 311–322 (2000).
24. J. Murai *et al*., Trapping of PARP1 and PARP2 by clinical PARP inhibitors. *Cancer Res.* **72**, 5588–5599 (2012).
25. D. Ahel *et al*., Poly(ADP-ribose)-dependent regulation of DNA repair by the chromatin remodeling enzyme ALC1. *Science* **325**, 1240–1243 (2009).
26. A. J. Gottschalk *et al*., Poly(ADP-ribosyl)ation directs recruitment and activation of an ATP-dependent chromatin remodeler. *Proc. Natl. Acad. Sci. U.S.A.* **106**, 13770–13774 (2009).
27. A. Pines *et al*., PARP1 promotes nucleotide excision repair through DDB2 stabilization and recruitment of ALC1. *J. Cell Biol.* **199**, 235–249 (2012).
28. D. Toiber *et al*., SIRT6 recruits SNF2H to DNA break sites, preventing genomic instability through chromatin remodeling. *Mol. Cell* **51**, 454–468 (2013).
29. H. Wong *et al*., Antitumor activity of targeted and cytotoxic agents in murine subcutaneous tumor models correlates with clinical response. *Clin. Cancer Res.* **18**, 3846–3855 (2012).
30. Z. Mao, Y. Jiang, X. Liu, A. Seluanov, V. Gorbunova, DNA repair by homologous recombination, but not by nonhomologous end joining, is elevated in breast cancer cells. *Neoplasia* **11**, 683–691 (2009).
31. Cancer Genome Atlas Research Network, Comprehensive and integrative genomic characterization of hepatocellular carcinoma. *Cell* **169**, 1327–1341.e23 (2017).
32. E. M. Kass *et al*., Double-strand break repair by homologous recombination in primary mouse somatic cells requires BRCA1 but not the ATM kinase. *Proc. Natl. Acad. Sci. U.S.A.* **110**, 5564–5569 (2013).
33. E. M. Kass, P. X. Lim, H. R. Helgadottir, M. E. Moynahan, M. Jasin, Robust homology-directed repair within mouse mammary tissue is not specifically affected by Brca2 mutation. *Nat. Commun.* **7**, 13241 (2016).
34. C. C. Chen *et al*., ATM loss leads to synthetic lethality in BRCA1 BRCT mutant mice associated with exacerbated defects in homology-directed repair. *Proc. Natl. Acad. Sci. U.S.A.* **114**, 7665–7670 (2017).
35. A. C. Begg, F. A. Stewart, C. Vens, Strategies to improve radiotherapy with targeted drugs. *Nat. Rev. Cancer* **11**, 239–253 (2011).
36. Y. Matsuda *et al*., DNA damage sensor γ -H2AX is increased in preneoplastic lesions of hepatocellular carcinoma. *ScientificWorldJournal* **2013**, 597095 (2013).
37. Y. Liu, A. Beyer, R. Aebersold, On the dependency of cellular protein levels on mRNA abundance. *Cell* **165**, 535–550 (2016).
38. M. J. O'Connor, Targeting the DNA damage response in cancer. *Mol. Cell* **60**, 547–560 (2015).
39. D. L. Hughes, Patent review of manufacturing routes to recently approved PARP inhibitors: Olaparib, rucaparib, and niraparib. *Org. Process Res. Dev.* **21**, 1227–1244 (2017).
40. D. M. MacAlpine, G. Almouzni, Chromatin and DNA replication. *Cold Spring Harb. Perspect. Biol.* **5**, a010207 (2013).
41. D. Davidson, L. Amrein, L. Panasci, R. Aloyz, Small molecules, inhibitors of DNA-PK, targeting DNA repair, and beyond. *Front. Pharmacol.* **4**, 5 (2013).
42. N. S. Gavande *et al*., DNA repair targeted therapy: The past or future of cancer treatment? *Pharmacol. Ther.* **160**, 65–83 (2016).
43. Z. Mao, A. Seluanov, Y. Jiang, V. Gorbunova, TRF2 is required for repair of non-telomeric DNA double-strand breaks by homologous recombination. *Proc. Natl. Acad. Sci. U.S.A.* **104**, 13068–13073 (2007).